DOI: 10.1002/marc.((insert number)) ((or ppap., mabi., macp., mame., mren., mats.))

Full Paper

Tomography of Electrospun Carbon Nanotube Polymeric Blends by Focus Ion Beam: Alignment and Phase Separation Analysis from Multicontrast Electron Imaging [1]

Eva M. Campo*, Douglas Yates, Benjamin Berson, Wudmir Rojas, W. Douglas Winter, Mohan Ananth, Jorge J. Santiago-Aviles, and Eugene M. Terentjev

_____

Prof. Eva M. Campo, Dr. Douglas Yates
Laboratory for the Research on the Structure of Matter University of Pennsylvania, Philadelphia, 19104, USA
E-mail: evamcampo@gmail.com

Benjamin Berson
Department of Electrical and Systems Engineering, University of Pennsylvania, Philadelphia, 19104, USA

Wudmir Rojas, W. Douglas Winter,
School of Electrical Engineering, Bangor University
Bangor , LL57 1UT, UK

Dr. Mohan Ananth
Carl Zeiss Microscopy, LLC, Ion Microscopy Innovation Center
Peabody, 01960, USA

Prof. Jorge J. Santiago-Aviles
Department of Electrical and Systems Engineering, University of Pennsylvania, Philadelphia, 19104, USA

Prof. Eugene Terentjev
Cavendish Laboratory, University of Cambridge,
Cambridge CB3 0HE, UK

_____

[1] **Supporting Information** ((bold)) is available online from the Wiley Online Library or from the author.

Multimodal focus ion beam (FIB) imaging on a Polydimethylsiloxane | Poly(methyl methacrylate)| Multiwall carbon nanotube (MWCNT) electrospun composite has been applied to discriminate the phase-separated polymer blend and identify MWCNT fillers. Upon tomographic reconstruction, this discrimination has been possible trough both atomic number and voltage contrast, the latter enabled by preferential MWCNT segregation to PMMA. This study suggests that electrospinning could be affecting not only MWCNT alignment, but also phase separation dynamics of immiscible polymers, yielding a porous structure throughout the fibers. This work opens the door to correlative materials science in polymer nanocomposites through FIB tomography, where voltage contrast is a main actor.

FIGURE FOR ToC_ABSTRACT

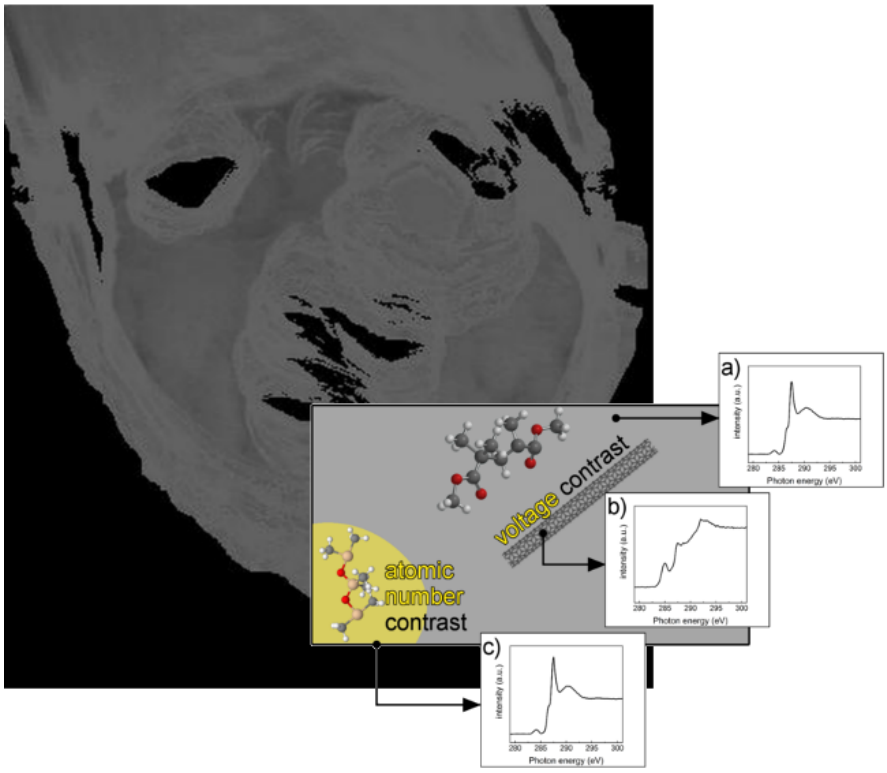

1. Introduction

Carbon nanotube polymeric composites are the focus of thorough studies as they improve on mechanical, thermal, and electrical properties of pristine polymeric systems. A crucial factor hindering subsequent technological applications is the tendency of nanofillers to bundle and entangle, producing defects in the composite and limiting performance efficiency.[1] In particular, dispersion and alignment of nanofillers are believed to unlock dynamical properties, key to highly innovative phenomena such as mechanical actuation and plasmonics.[2, 3] Previously, we have demonstrated correlation between processing and alignment through synchrotron and Raman spectroscopies as well as Atomic Force and Helium Ion microscopies[4] in the context of structural,[5] and smart (i.e. mechanically actuating) systems.[6, 7]

In fact, on those earlier reports, we have discussed the impact that electrospinning bears on both carbon nanotube (CNT) alignment and bonding dynamics.[5] Indeed, electrospinning has proven successful in the promotion of dispersion and alignment of CNTs in polymeric composites. [8]

On those lines, dispersion of CNTs can be routinely documented through transmission electron microscopy (TEM) techniques and surficial CNTs can be assessed by a variety of microcopy techniques such as scanning electron microscopy (SEM) and more recently through He-Ion Microscopy, as seen in **Figure 1**. However, characterization routines that allow for direct inspection of CNT alignment in the bulk, at the tens of microns length scales, are still under development at this time.

In recent years, tomographic TEM, focus ion beam (FIB), and X-Ray technologies have enabled workflows covering sub-nanometer to tens of microns voxel sizes (i.e.

volumetric resolution) and analyzed volumes ranging from $(10\ nm)^3$ to $(10\ mm)^3$ (**Figure S1** in the Supporting Information).[9] The possibility of sequentially deploying the adequate technique to relevant regions of interest simultaneously addresses the problem of resolution and lengthscales paving the way into a new age in materials characterization: correlative imaging in materials science.[10]

Beyond atom probe, tomographic TEM features highest resolutions and smallest length scales[11] and the feasibility of analyzing CNT distribution in a quantitative fashion has been recently demonstrated.[12] However, a paramount draw back in the examination of filler dispersion by TEM is the lack of representation beyond the sectioned area, i.e. the problem of the length scale. In this scheme, a slab in the hundreds of nanometers is hardly representative of the dispersion of fillers even in the nearest vicinity of the extracted region, as nanoparticles can agglomerate in a rather inconsistent fashion. In trying to explore the dispersion and alignment of fillers beyond the immediate vicinity, many thinning sections would be needed, complicating analysis and increasing costs. On the larger length scales, sub-micrometer X-ray microscopy is enabling non-destructive nanoscale tomography in technologically relevant materials systems,[13] while augmenting the length scale beyond that of FIB's,[10] and enabling correlative microscopy workflows (Figure S1 in the Supporting Information). Albeit, the feasibility to image CNTs in a polymeric matrix has still not been demonstrated through X-ray microscopies. Notably, in the midsection of the resolution/length scale space, a number of soft matter and composite systems have been explored with FIB-tomography, such as bone-tissue interfaces.[14] However, the feasibility (and convenience) to observe CNTs upon FIB milling (owing to low contrast) has been debated in the context of CNTs embedded in mouse lung tissue.[15] Clearly, upon cross-section FIB milling, SE observation of

CNTs embedded in a polymeric-type matrix is complicated due to poor topographic and chemical information yielded by SE and BSE electrons respectively.

Albeit, given the importance of monitoring both phase separation and porosity in electrospun systems which have proven of technological avail in remediation,[16] cellular infiltration,[17] and enhanced electromechanical performance,[18] the study of electrospun systems through FIB tomographic approaches, is long due.

In light of this discussion, there is clear need to devise characterization schemes that offer localized details on dispersion and alignment suitable to be combined with ease to explore relevant regions of interest in CNT composites. In particular, what is called for is an imaging technique with resolving power in the tens of nanometers, capable of discerning contrast derived from the fine chemical/structural information enclosed at the CNT-polymer interface, and suitable to be deployed throughout tens of microns.

In this communication, we report on the feasibility of FIB tomography to study subsurface CNTs embedded in a polymeric matrix with the purpose of volumetric reconstruction. FIB tomography, despite its destructive nature, has the great built in advantage of allowing multiple imaging modes. This multiplicity results from the availability of a variety of secondary electron (SE) detectors, namely the conventional Everhart-Thornley (ET), as well as in lens and backscattered electron (BSE) detectors. In addition, multiple contrast is available within the SE-ET detector, capable of capturing effects from topography, channeling, and atomic number (through collection of BSE emitted within the solid angle tendered by the detector).[19] Here, we will demonstrate that field effects derived from localized e-matter interactions in distinctively conductive material systems also yield voltage-derived contrast, suitable for tomographic reconstruction.

2. Experimental Section

2.1 Composite synthesis and fiber processing through electrospinning

A polymeric blend containing PDMS and PMMA was assembled following the procedure reported earlier by Yang,[20] and unmodified MWCNTs were added to the mixture. As described in earlier procedures,[5] a solution prepared from 2.0365 grams of PMMA (molecular weight 210,000) 2.02 ml of Sylgard-184 PDMS with a molecular weight of ~60,000, 0.2ml of curing agent, 10 ml DMF, 10 ml THF, and 0.0083 grams of MWCNT was mixed and placed under magnetic stirring for two weeks and then sonicated and electrospun with the following parameters: 8kV, 5 cm distance, and 0.5 ml/s It was spun onto a rotating drum to align the fibers. The MWCNTs used here were purchased from Nanostructured & Amorphous Materials, Inc.; Houston, TX 77084, USA, purity higher than 95 %, a surface area of 64 m^2/g, and an outside diameter in the range of 60 to 80 nm with lengths around 15 μm.

2.2 Characterization

Untreated MWCNTs were characterized using a JEOL JEM-2010F field-emission operated at 200 kV, and a JEOL JEM-ARM200F electron microscope. STEM images were simultaneously recorded in both the High Angle Annular Dark Filed (HAADF) and Bright Field (BF) modes at 80 kV. Probe correction was performed with a CEOS corrector obtaining a twelve-fold Ronchigram with a flat area of ~40 mrad. Images were registered with a condenser lens aperture of 30 microns (convergence angle 25 mrad), and HAADF collection angle ranged from 45 to 180 mrad. Spot size used was ~35 pA.

The untreated fibers were imaged in an ORION Plus He-IM Zeiss at 35kV with the assistance of a flood gun to prevent surface charging.

NEXAFS spectra were collected at the Carbon K-edge in partial electron yield mode at U7A beamline, NSLS, BNL, using a horizontally polarised beam of 2mm in diameter. Charging of the polymeric samples was prevented by using a flood gun during acquisition. Energy resolution for NEXAFS acquisition was 0.1 eV. NEXAFS spectra were then normalised using the Athena software.

A sample of the film was sputter-coated with Au-Pd for 30 seconds at 0.08 mb one week after spinning, and analyzed with an FEI Strata DB235 SEM/Focused Ion Beam (FIB) with Auto Slice & View™ software.

2.3 Milling sequence- Data Treatment- Image reconstruction

Using a dual beam focused ion beam (FIB), it is possible to create reconstructions of structures through tomography. Indeed, after FIB dissecting, collected images from milled sections can be stacked to produce a three dimensional dataset.

We followed the procedure detailed by Holzer.[21] Briefly, using the SEM, we located a fibers angled vertically out of the sample to allow for perpendicular milling. Perpendicular milling is preferred for convenience in revealing the internal structure of the fiber, as well as embedded CNTs, and any other subsurface features. The sample is placed at the eucentric point where the two columns converge at an angle of 52°. Hence, while the ion beam can be used for precise sample manipulations (milling, cutting, polishing), the sectioned planes can be imaged in SEM mode. The principal geometry is shown in Figure S2. During the serial sectioning process, the stage tilt is kept constant at 52°.

In the depicted scheme, the sample surface (x–y plane) is perpendicular to the ion beam (z-direction). The FIB-prepared imaging planes are defined as x–z planes and their intersection with the sample surface as the x-direction. Secondary electron (SE) images of the x–z planes are taken from an angle of 52°.

During the sectioning procedure, a series of layers are now milled away with a constant thickness in the y-direction.

An exploration was needed to determine ideal irradiation conditions both for milling and imaging, given the soft nature of the material system under study, prone to irradiation damage and generation of artifacts. [22]Using automatic feature at the FEI Strata (Slice and View), we test-milled an area of X=20 μm, Y = 3 μm, Z = 1 μm using the silicon material file "si.mtr", The I-beam was set at 500 pA for the milling procedure. Images were taken of the sliced fiber, and the E-beam was at 3 KV during SE image recording. These test milling conditions effectively milled the fiber through its depth (on the order of 10 μm) since the milling file had been calibrated for Si, with larger stopping power. Upon testing the optimum milling conditions, we defined a new geometry for sample milling.

The automated process featured by "Slice and View" was programmed to mill a total of 20 slices into the Y-axis of the other fiber. The dimensions of the three-dimensional cut were X=16 μm, Y = 10 μm, Z = 1 μm. A few of the initial tomographs were discarded as they milled debris from the intitial cross-section. On ten consecutive images (yielding a cross-section stack 5 μm long), the background was cropped and cavities were also cropped through their internal perimeter, using GIMP-GNU free photo editing software. Using freely available Image J/FIJI,[23] a three-dimensional imaging software, we imported the slices as an image sequence.

Under the "Analyze" menu, the tomographs were calibrated (with assistance from a calibrated SEM image).

The slice spacing was set to 0.5 microns to ensure fidelity in reproducing the volume, with opacity set to 5%. Surface depth-cueing, interior depth cueing, upper transparency bound and lower transparency bound were set to 100%, 50%, 100, and 4, respectively. The rotation angle increment was set to 1 and the projection method was "brightest point." An interpolated, rotating three-dimensional visualization of the fiber was created using the "3D Project" function available in the "stacks" menu. Finally, staking of modified images yielded the tomographs shown in Figure 3a and 3b, as well as the animations in SI II. Two rotating images were created, one about the X-axis and one about the Y-axis. We also colored the image for easier viewing

3 Results and Discussion

Transmission electron microscopy of the CVD-grown MWCNTs used in this work is shown in Figure 1a and 1b, revealing distribution size in the order of 60-80 nm in diameter and multiple defects across the graphitic lattice. The untreated CNTs were embedded in a PDMS-PMMA blend to fabricate electrospun fibers (Figure 1c). Prior works suggest that the combined action of extrusion and electric forces in electrospinning, can induce CNT alignment within single fibers,[24-26] as revealed through AFM imaging upon polymer calcination,[8] through direct TEM inspection on nm-thick fibers, [27] and by TEM tomography.[28]

The chemistry of choice in this work is a blend of Polydimethylsiloxane *(*PDMS) and Poly(methyl methacrylate) *(*PMMA). Both polymers are independently rightful

technological systems,[29] with abundant presence in microfluidics and MEMS, owing to excellent tribology properties. As a tandem, the possibility of combining hydrophobic polymers featuring distinct mechanical properties, has promoted investigations to control this naturally-occurring phase separation.[30] In this context, the larger molecular mass of PMMA provides a vehicle for PDMS to be electrospun. Details of the fabrication are included in the Supporting Information.

The resulting fibers showed cylindrical and ribbon morphologies (Figure 1c and d), with diameters ranging in the tens of microns. Metal-coated fibers were imaged in vacuum under SE mode, revealing surficial CNTs, aligned parallel to the surface. Some CNTs are also observed protruding from the cross-section (figure 1c). Uncoated fibers were also imaged by He-ion microscopy (Figure 1d), revealing previously unreported rippling contrast from the vicinity of surficial CNTs, whose origin has been attributed to drag effects of CNTs on the matrix upon collection.[4] In fact, this rippling effect is observed topographically in HIM, as a consequence of preferential segregation of CNTs to PMMA in the electrospun fibers. This is a crucial finding that will be useful in the discussion of mechanism responsible for CNT contrast in upcoming sections.

3.1. Milling sequence

Serial sectioning was conducted on a FEI-FIB Dual Beam Strata following standard reported procedures (**Figure S2** of the Supporting Information), with FEI's commercially available software Slice and View, followed by data processing and reconstruction of the 3D structures. Importantly, sectioning was conducted on a single stand-alone fiber. Sequential, as-acquired e-beam images through the Everhart-Thornley detector (**Figure 2**) show no evidence of material redeposition or random electrical charging from either ion or electron beam irradiation, justifying stacking

towards image reconstruction. A detailed discussion of possible ion and electron beam-induced artifacts is provided in SI. Indeed, earlier studies on electron and ion beam- induced damage, had reported the possibility of modified functional chemistry at local level in soft systems.[22] Modified chemistries ranged from molecular effects (hydrogen loss and local modification of bonding type amongst nearby species) to the generation of a thin surficial contamination layer. However, none of those would be detected by SE or HIM imaging, but through more sensitive synchrotron spectroscopies (see Section 2.1 in the Supporting Information). We conclude that the tomograms assembled are artifact-free, and this point will be discussed further during contrast analysis.

3.2 Multicontrast imaging to address phase separation and topography

Images of the reconstructed single fiber point at a cavernous structure-that was confirmed further by the stacking of sequential tomograms (**Figure S3** in the Supporting Information), featuring a labyrinth of pores seemingly propagating parallel to the fiber axis. The other obvious contrast corresponds to the expected micro-phase separation between PDMS and PMMA, known to develop through non-equilibrium thermodynamics in un-annealed films, due to the difference in hydrophobicity of both components in the blend.[31] Phase separation is a known effect in immiscible polymeric blends, and this study suggests FIB tomography is a suitable tool to monitor the evolution of phase separation through the bulk, taking advantage of multicontrast electron imaging.[19] The availability of a SE detector capable of collecting both SE and backscattered electrons (BSE) emitted within the collection angle of the ET detector, enables the differentiation of PDMS, with higher

BSE emission efficiency owing to the presence of a higher atomic weight element (Si) in the backbone.

Importantly, ES has had a different effect on the dynamics of phase distribution than reported earlier. Indeed, bright areas in electron microscopy images in Figure 2, are confined to island-like regions with sizes varying between the micron and the sub-micron scale. Notably, the 10 μm-wide fiber confers PMMA a dominant matrix role, where PDMS phase separates, contrary to the expected behavior where the more hydrophobic PDMS, i.e. lower surface energy, surfaces to the vacuum or air-sided interfaces.[30, 32] We attribute these differences to effects derived from the electrospinning process, where surface tension, viscosity and conductivity are affecting phase separation dynamics. In particular, it is proposed that lack of molecular entanglement which confers PDMS a secondary role and this is likely the reason for segregation within PMMA.

In addition, the question arises per the possibility of electrospinning arising from possible macromolecule alignment.[33-35] However, for this system, alignment has been thoroughly discussed in early works through synchrotron spectroscopies. Dichroic ratio studies suggested that macromolecules did not align, which is consistent with the referred works, since no additional electric field was used upon collection.[5]

Sequential FIB milling had been applied earlier in a subsurface investigation of meteoritic particles to reveal a porosity structure as well as phase separated components, which were imaged in BSE mode.[22] That procedure was without prejudice to chemical and morphological analysis of ceramic and metal agglomerates. The question arises to whether the observed contrast mechanism behind phase separation is legitimate and not the consequence of irradiation-derived artifacts. A

detailed discussion to this effect is provided in the Supporting Information, confirming the absence of such artifacts here (section S1.1).

3.3. Image reconstruction

Sequential sectioning produced a library of SE tomograms (Figure S3) Visualization of the milling sequence suggested some contrast vaguely pointing at the presence of CNTs (Figure S3 in the Supporting Information) Since stacking of unmodified image slices would not offer any additional information due to the lack of transparency from each tomogram, a digital image treatment was envisioned, that is detailed in the Supporting Information. The resulting tomographic reconstruction is shown in **Figure 3**. In addition, animations with the x and y rotation of the reconstructed fiber, can be found in the supplementary animation files SA1 and SA2 respectively (multimedia view……..). The resulting volume reconstructions successfully displayed phase separation as detailed in the Supporting Information. Upon reconstruction, phase separation, pores, and, interestingly, filamentous contrast are discriminated. Contrast from the filament-shaped structures is bright, and line scan profiles reveal thickness in the order of 100 nms. We attribute the filamentous contrast to CNTs that have not fully aligned parallel to the fiber due to their short length. This result been consistent with prior findings by Dror et al. that confirmed poor CNT alignment in some electrospun fibers through direct TEM observation.[27] Albeit, both surficial and embedded longer CNTs are preferentially aligned parallel to the fiber, as seen in Figures 1c and d.

3.4 Mechanism responsible for CNT contrast

We now explore the rationale responsible for CNTs contrast. We had proven earlier that CNTs have preferentially segregated to the PMMA phase (the darker contrast being associated to lower atomic number) through synchrotron spectroscopy,[5] as well as by free energy considerations and further confirmed through Helium microscopy,[4] as summarized in **Figure 4**. Selective migration of CNTs to PMMA rich areas further supports the notion of the porous structure not being a result of CNTs presence, but rather to the phase separation dynamic in a confined micro fiber.

Since neither topographic (freshly cleaved interfaces) or atomic number differences (CNTs and PMMA are mostly C-rich systems) seem feasible, we propose voltage contrast as the mechanism conducive to CNT observation, as shown in Figure 4. Voltage contrast (VC) upon e-beam irradiation was first deployed in metal-insulator interfaces,[36] and has already been used to analyze CNT/polymer interfaces both in the two modalities, where the substrate is being biased, [37, 38] as well as with no bias.[39]

The origin of this contrast is voltage induced, due to differences in the relative conductivity of CNTs and PMMA,[40] where sampling depths are quoted in the range of 20 nm, providing some level of subsurface image capability, also as a function of electron beam voltage.[39] In fact, a detailed analysis on CNT imaging on a polymeric matrix has been conducted by Kovacs and co-workers,[41] where, electron beam changes in voltage, current density, and irradiation time led to visualization of CNTs in the matrix due to induced VC. In this case, the CNTs are charging negatively, promoting excess SE emission. In this context, relative contrast sign and conductivity difference between PMMA and CNTs upon ion beam irradiation are discussed in the Supporting Information (sections S1.2 and S1.3 respectively), as they conveniently aid in the observation of CNTs.

Notably, Loos reported the nominal 3nm diameter SWCNTs in their study showed a 30 nm diameter when imaged through VC.[39] Similarly, Kovacs could image original 15 nm diameters SWCNT as bright features of 30 nms diameter.[41] This has been attributed to local charging of the polymer surrounding the imaged CNTs. On the same lines, the nominal 60-80 nm diameter MWCNTs used in this study, reveal a diameter of 100 nms when imaged by virtue of VC mechanisms.

We attribute the visibility of CNTs in this system to two factors. First, the CNTs preferentially segregated to the PMMA phase, as confirmed by synchrotron spectroscopy[5] and He Ion microscopy,[4] conferring enough conductivity difference with MWCNTs for excess charge-generated during the e-beam imaging process be confined within the CNTs and the immediate vicinity. Under the current irradiation conditions, electron confinement produced an excess SE emission upon further irradiation. In addition, despite the dominant PMMA nature of the electrospun fibers, these were metal-coated, and the 10-um diameter confers an adequate path to ground, granting an overall electrically stable system, suitable of being imaged by preventing undesirable charging artifacts. In this scheme, charge is being confined at the CNT/polymer interface to produce a VC suitable to image CNTs without detriment to the overall electrical stability of the system, that can be legitimately monitored through SE imaging. And it is precisely the leaking of this charge what confers CNTs with larger diameters, of up to an order of magnitude difference. [39]

We have attributed the filamentous contrast to CNTs that have not fully aligned parallel to the fiber due to their short length. Long CNTs in the bulk are preferentially aligned parallel to the fiber, as seen in Figures 1 c and d. This is consistent with other works, were ES polymer nanocomposites also observed CNTs as preferentially parallel to the fiber.[24] In addition, it is worth highlighting that HIM and

thermodynamical arguments confirm that CNTs have preferentially segregated to the PMMA phase, and hence, their alignment is irrespective of phase separation. Regarding spatial distribution of nanofillers, TEM works have already confirmed CNTs don't systematically align in electrospun fibers.[27] In addition, given the different molecular conformability observed by Camposeo et al., inhomogeneities on the CNT alignment can also be expected.[42] In this particular scenario, we speak of preferential alignment and further work is needed to understand CNT alignment in electrospinning to address overall distribution and inhomogeneous orientations.

4. Conclusions

We have shown FIB tomography is a suitable technique to monitor both phase separation and porosity in electrospun systems. This work emphasizes the value of FIB tomography in CNT polymer composites towards correlative tomography, where MWCNTs are shown by virtue of voltage contrast, opening the door towards x-ray tomographic methods. Future validation of x-ray tomography in CNT nanocomposites will aim at closing the gap between light and electron microscopy in the realm of correlative imaging, bridging the nanometer to millimeter lenghtscales through multicontrast imaging afforded by Everhart-Thornley SE detectors, where atomic number and voltage contrast are the main actors.

Supporting Information

Supporting Information is available from the Wiley Online Library or from the author.

Acknowledgements:

We acknowledge funding from AFOSR Grants FA9550-15-1-0289, FA9550-14-1-0099, and AOARD travel grant under Window-On-Science (WOS) program. FP7 support from NMP 22896 and COST Action MP1206 EU on Electrospinning is also gratefully acknowledged.

This work made use of *MRSEC* Shared Experimental Facilities supported by the *National Science Foundation* under *Award No*. *DMR 96-32598 as well as PREM Shared Experimental Facilities under* Grant # DMR 0934218: "Alloys at the Nanoscale". Use of the National Synchrotron Light Source, Brookhaven National Laboratory, was supported by the U.S. Department of Energy, Office of Science, Office of Basic Energy Sciences, under Contract No. DE-AC02-98CH10886. Computational facilities are afforded through High Performance Computing Wales project numbers 095 and 224, as part of the HPCW-Project No. 80621, funded through the European Regional Development Funding.

Received: Month XX, XXXX; Revised: Month XX, XXXX; Published online:

((For PPP, use "Accepted: Month XX, XXXX" instead of "Published online")); DOI: 10.1002/marc.((insert number)) ((or ppap., mabi., macp., mame., mren., mats.))

Keywords: electrospinning, nanocomposites, focus ion beam, tomography

[1] M. Moniruzzaman, K. I. Winey, *Macromolecules* **2006**, *39*, 5194.

[2] S. V. Ahir, E. M. Terentjev, *Phys. Rev. Lett.* **2006**, *96*, 133902.

[3] P. Wang, L. Zhang, Y. Xia, L. Tong, X. Xu, Y. Ying, *Nano Lett.* **2012**, *12*, 3145.

[4] E. M. Campo, E. Larios, C. Huynh, M. Ananth, *J. Mater. Res.* **2015**, *30*, 130.

[5] A. D. Winter, F. M. Alamgir, C. Jaye, D. Fischer, E. M. Campo, *Langmuir* **2013**, *29*, 15882.

[6] A. D. Winter, K. Czaniková, E. Larios, V. Vishnyakov, C. Jaye, D. A. Fischer, M. Omastová, E. M. Campo, *J. Phys. Chem. C* **2015**, *119*, 20091.

[7] A. D. Winter, E. Larios, F. A. Alamgir, C. Jaye, D. Fischer, M. Omastová, E. M. Campo, *J. Phys. Chem. C* **2014**.

[8] J. Gao, A. Yu, M. E. Itkis, E. Bekyarova, B. Zhao, S. Niyogi, R. C. Haddon, *J. Am. Chem. Soc.* **2004**, *126*, 16698.

[9] M. D. Uchic, L. Holzer, B. J. Inkson, E. L. Principe, P. Munroe, *MRS Bulletin* **2007**, *32*, 408.

[10] L. L. Arno P. Merkle, Andy Steinbach, Jeff Gelb, Martin Kienle, Michael W. Phaneuf, David Unrau, Sudhanshu S. Singh and Nikhilesh Chawla, *Microscopy and Analysis* **2014**, *7*, 10.

[11] K. J. Batenburg, S. Bals, J. Sijbers, C. Kübel, P. A. Midgley, J. C. Hernandez, U. Kaiser, E. R. Encina, E. A. Coronado, G. Van Tendeloo, *Ultramicroscopy* **2009**, *109*, 730.

[12] B. Natarajan, N. Lachman, T. Lam, D. Jacobs, C. Long, M. Zhao, B. L. Wardle, R. Sharma, J. A. Liddle, *ACS Nano* **2015**, *9*, 6050.

[13] H. E. Misak, S. Mall, *Carbon* **2014**, *72*, 321.

[14] L. A. Giannuzzi, D. Phifer, N. J. Giannuzzi, M. J. Capuano, *Journal of Oral and Maxillofacial Surgery*, *65*, 737.

[15] C. Købler, A. T. Saber, N. R. Jacobsen, H. Wallin, U. Vogel, K. Qvortrup, K. Mølhave, *Anal. Bioanal. Chem.* **2014**, *406*, 3863.

[16] H. Dong, P. H. Gary, S. Brian, C. B. Scott, "Electrospun and Oxidized Cellulosic Materials for Environmental Remediation of Heavy Metals in Groundwater", in *Model Cellulosic Surfaces*, American Chemical Society, 2009, p. 243.

[17] J. B. Lee, S. I. Jeong, M. S. Bae, D. H. Yang, D. N. Heo, C. H. Kim, E. Alsberg, I. K. Kwon, *Tissue Engineering Part A* **2011**, *17*, 2695.

[18] Z. Jian, G. Qiang, F. Tadashi, S. Hirofusa, K. Mutsumi, *Nanotechnology* **2011**, *22*, 275501.

[19] L. A. Giannuzzi, "Multi-signal FIB/SEM tomography", in *SPIE Defense, Security, and Sensing*, International Society for Optics and Photonics, 201283780P.

[20] D. Yang, X. Liu, Y. Jin, Y. Zhu, D. Zeng, X. Jiang, H. Ma, *Biomacromolecules* **2009**, *10*, 3335.

[21] L. Holzer, F. Indutnyi, P. Gasser, B. Münch, M. Wegmann, *Journal of Microscopy* **2004**, *216*, 84.

[22] N. Bassim, B. De Gregorio, A. Kilcoyne, K. Scott, T. Chou, S. Wirick, G. Cody, R. Stroud, *Journal of Microscopy* **2012**, *245*, 288.

[23] C. A. Schneider, W. S. Rasband, K. W. Eliceiri, *Nat Meth* **2012**, *9*, 671.

[24] F. Ko, Y. Gogotsi, A. Ali, N. Naguib, H. Ye, G. Yang, C. Li, P. Willis, *Adv. Mater.* **2003**, *15*, 1161.

[25] H. Hou, J. J. Ge, J. Zeng, Q. Li, D. H. Reneker, A. Greiner, S. Z. Cheng, *Chem. Mater.* **2005**, *17*, 967.

[26] L.-Q. Liu, M. Eder, I. Burgert, D. Tasis, M. Prato, H. D. Wagner, *Appl. Phys. Lett.* **2007**, *90*, 083108.

[27] Y. Dror, W. Salalha, R. L. Khalfin, Y. Cohen, A. L. Yarin, E. Zussman, *Langmuir* **2003**, *19*, 7012.

[28] T. Vad, J. Wulfhorst, T.-T. Pan, W. Steinmann, S. Dabringhaus, M. Beckers, G. Seide, T. Gries, W. F. C. Sager, M. Heidelmann, T. E. Weirich, *Macromolecules* **2013**, *46*, 5604.

[29] N. S. Tambe, B. Bhushan, *Ultramicroscopy* **2005**, *105*, 238.

[30] H. Chen, X. Deng, X. Hou, R. Luo, B. Liu, *Journal of Macromolecular Science, Part A* **2008**, *46*, 83.

[31] M. Harris, G. Appel, H. Ade, *Macromolecules* **2003**, *36*, 3307.

[32] K. Lian, C. Chen, H. Liu, N. Wang, H. Yu, Z. Luo, *J. Appl. Polym. Sci.* **2011**, *120*, 156.

[33] M. V. Kakade, S. Givens, K. Gardner, K. H. Lee, D. B. Chase, J. F. Rabolt, *J.Am.Chem.Soc.* **2007**, *129*, 2777.

[34] S. Pagliara, M. S. Vitiello, A. Camposeo, A. Polini, R. Cingolani, G. Scamarcio, D. Pisignano, *J. Phys. Chem. C* **2011**, *115*, 20399.

[35] M. Richard-Lacroix, C. Pellerin, *Macromolecules* **2013**, *46*, 9473.

[36] W. R. Bottoms, D. Guterman, P. Roitman, *Journal of Vacuum Science & Technology* **1975**, *12*, 134.

[37] V. Aravind, Y. T. Marina, G. Kestutis, G. N. Albert, I. K. Esko, K. Ralph, *Nanotechnology* **2011**, *22*, 265715.

[38] A. Vijayaraghavan, Blatt, S., Marquardt, C., Dehm, S., Wahi, R., Hennrich, F., & Krupke, R., *Nano Research* **2008**, *4*, 321.

[39] J. A. Loos, A. Grossiord, N. Koning, C. E., Regev, O., *Ultramicroscopy* **2005**, *104*, 160.

[40] F. Du, J. E. Fischer, K. I. Winey, *Journal of Polymer Science Part B: Polymer Physics* **2003**, *41*, 3333.

[41] J. Z. Kovacs, K. Andresen, J. R. Pauls, C. P. Garcia, M. Schossig, K. Schulte, W. Bauhofer, *Carbon* **2007**, *45*, 1279.

[42] A. Camposeo, I. Greenfeld, F. Tantussi, M. Moffa, F. Fuso, M. Allegrini, E. Zussman, D. Pisignano, *Macromolecules* **2014**, *47*, 4704.

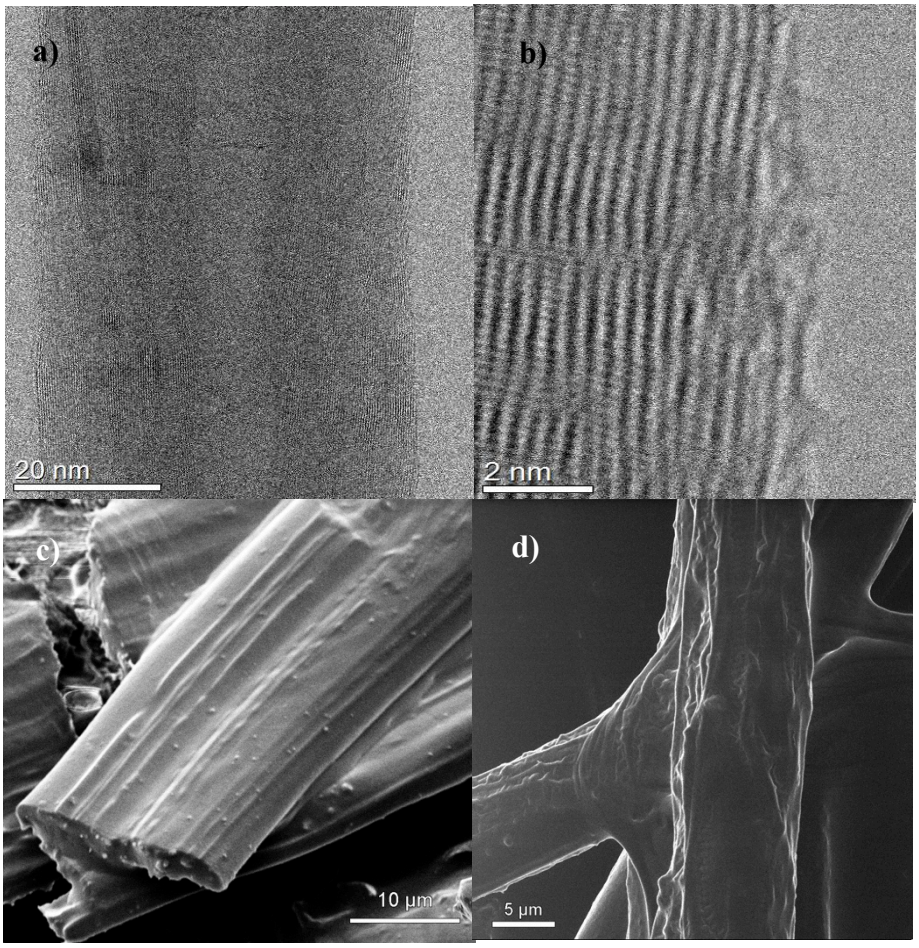

Figure 1. ((a) and b) TEM images of MWCNTs used in this study, c) SEM, and d) HIM images of electrospun fibers))

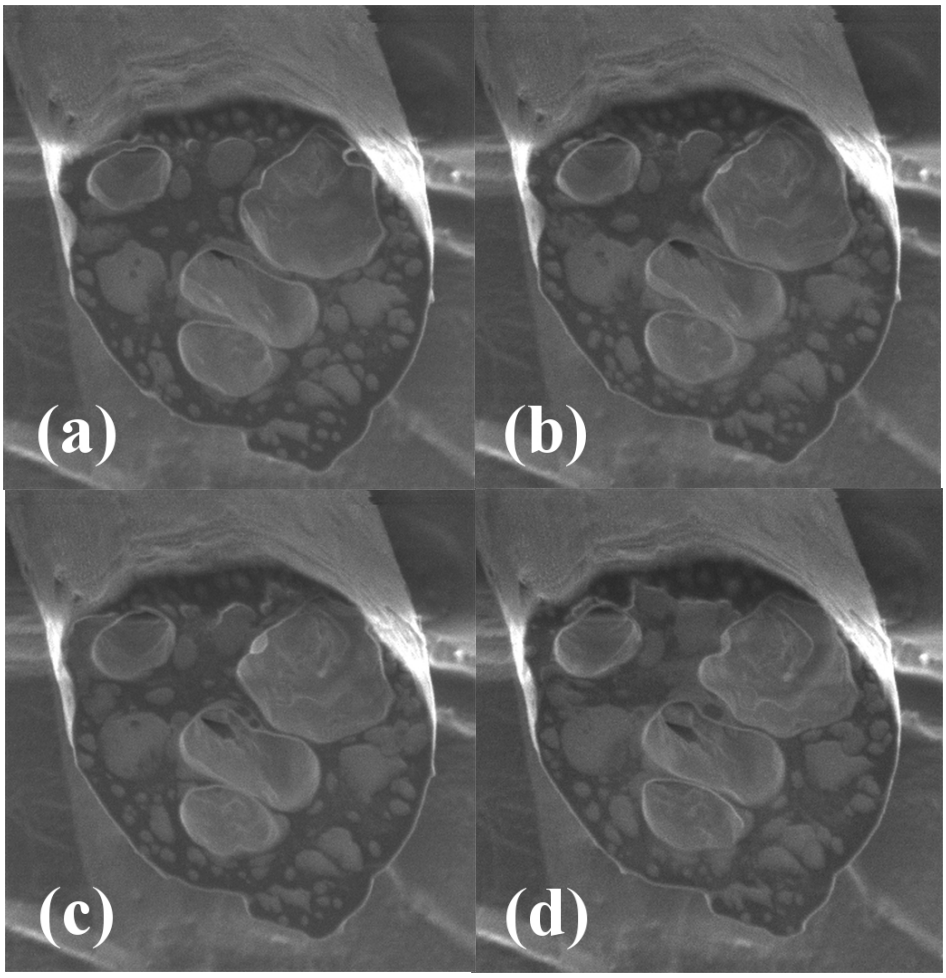

Figure 2. ((a), b), c) Set of sequential tomograms acquired upon sequential milling of a single fiber, a), b), c) d). The diameter of the fiber is 10μm. Tomograms reveal absence of material redeposition upon milling.))

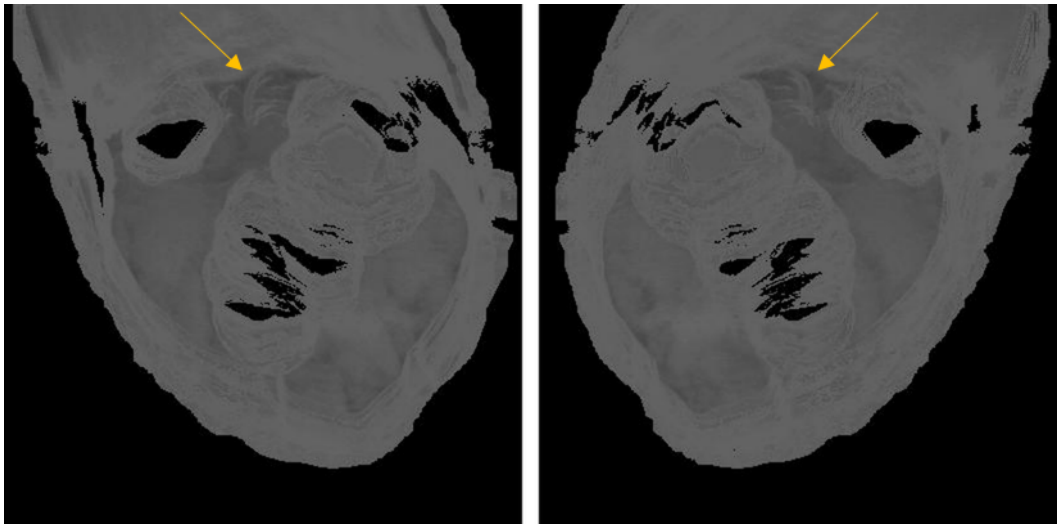

Figure 3. ((Tomographic reconstruction of a single fiber in grey scale showing front (left) and back (right) views of the reconstructed tomograms. Bright regions are a consequence of all topographic, atomic number, and voltage contrast. A filamentous contrast is observed in the upper center region of the fibers (shown by arrows) which was previously unresolved from the individual tomograms, given its oblique directional distribution with respect to the milling direction.))

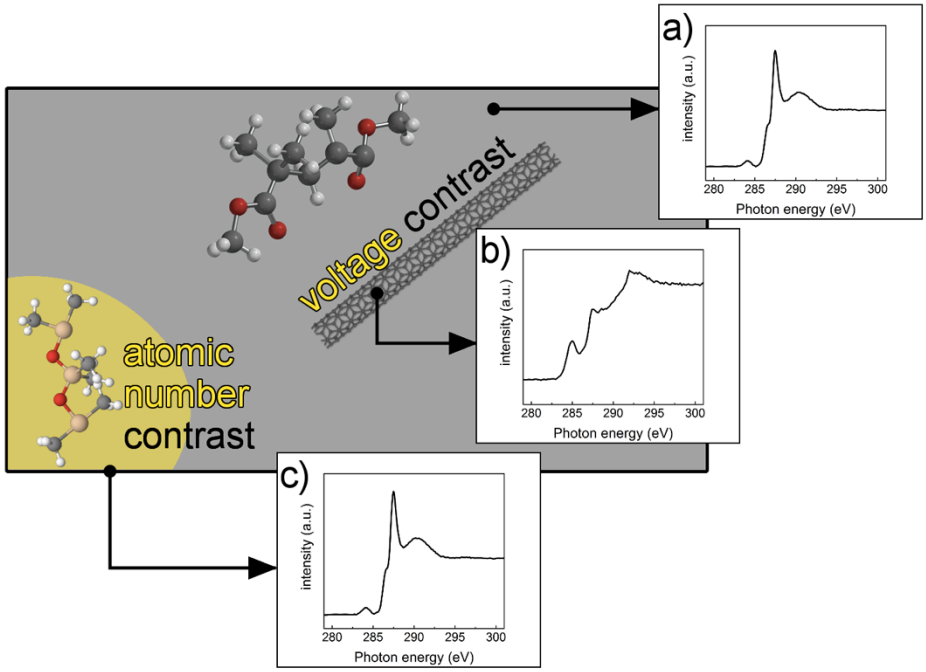

Figure 4. ((Figure Caption. Schematic summarizing the types of contrast present in this study, where NEXAFS spectra a), b), and c) correspond to PMMA, MWCNT, and composite respectively. [5] It can be seen that the spectra in c) corresponds mostly to the fingerprint of PMMA in a), and the MWCNTs have preferentially migrated to the PMMA phase. [4]))

The value of FIB tomography is highlighted to discern phase separation, CNT alignment, and porosity in electrospun fibers. Framed in the context of correlative tomography, this work is a proof of concept on the viability of FIB tomography in nanocomposites. The value of this technique is further highlighted in electrospinning, where inhomogeneities are likely to develop throughout a fiber.

Eva M. Campo*, Douglas Yates, Benjamin Berson, Wudmir Rojas, W. Douglas Winter, Mohan Ananth, Jorge J. Santiago-Aviles, and Eugene M. Terentjev.
Corresponding Author*

Tomography of electrospun Carbon Nanotube Polymeric blends by Focus Ion Beam: Alignment and Phase Separation Analysis from Multicontrast Electron Imaging

ToC figure

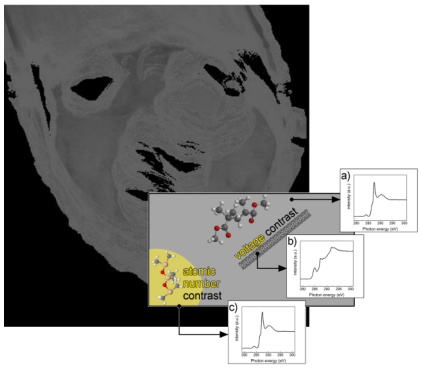

((Supporting Information should be included here for submission only; for publication, please provide Supporting Information as a separate PDF file.))

Supporting Information

for *Macromol. Mater. Eng.*, DOI: 10.1002/mame.2013#####

Tomography of Electrospun Carbon Nanotube Polymeric Blends by Focus Ion Beam: Alignment and Phase Separation Analysis from Multicontrast Electron Imaging
Title of Manuscript[2]

Eva M. Campo*, Douglas Yates, Benjamin Berson, Wudmir Rojas, W. Douglas Winter, Mohan Ananth, Jorge J. Santiago-Aviles, and Eugene M. Terentjev

[2] **Supporting Information** ((bold)) is available online from the Wiley Online Library or from the author.

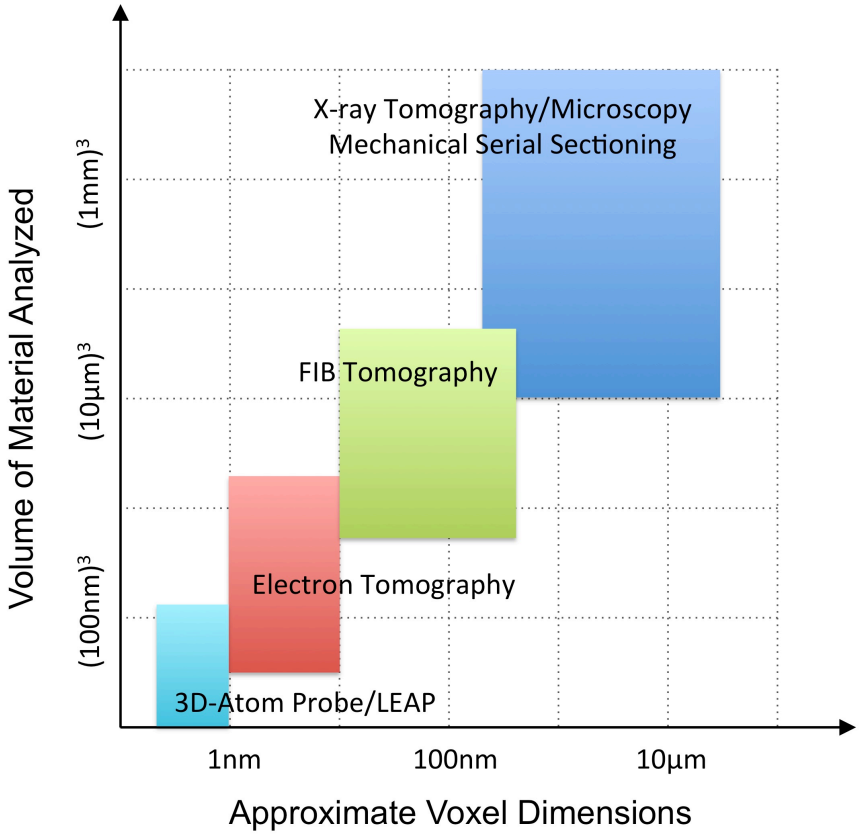

Figure S1: instrumentation/technique domains in the correlative microscopy flow currently available in the tomography realm. Polymer nanocomposites so far, had not been studied by X-ray Tomography or FIB tomography successfully. Adapted after Uchic[1] and Merkle.[2]

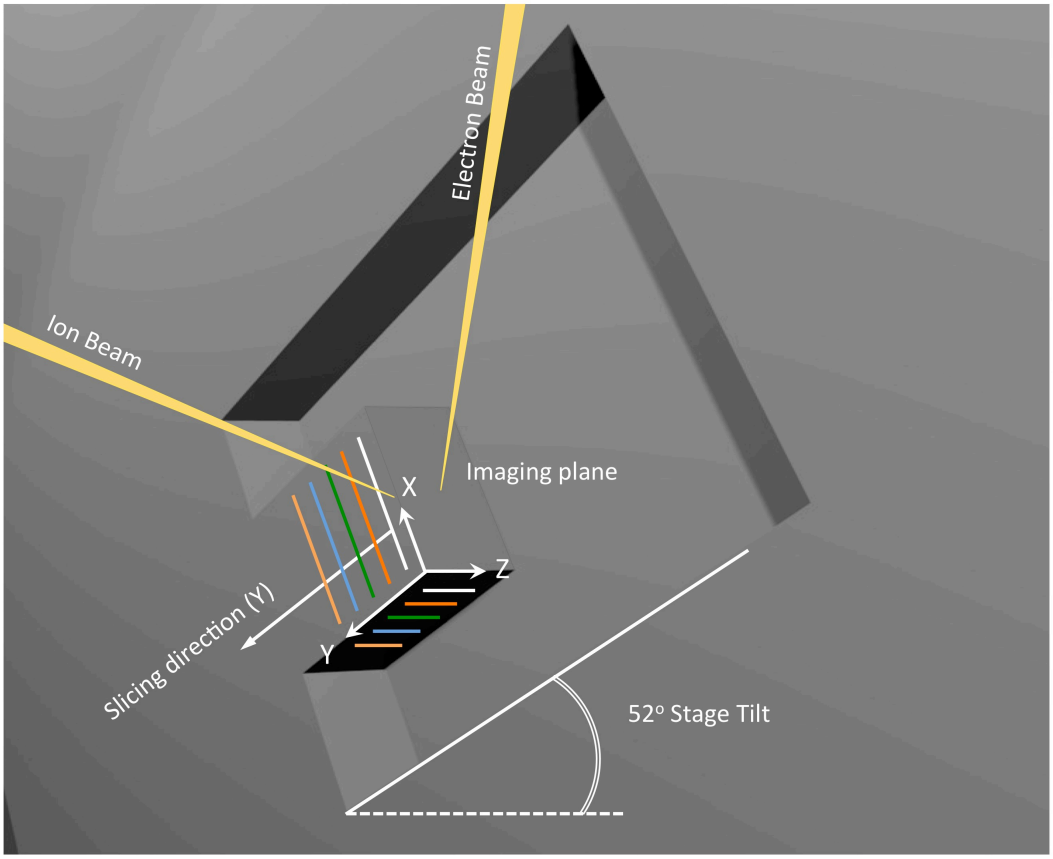

Figure S2: Architecture behind sample milling suitable for tomographic reconstruction. Modified from Holzer[3]

3 Further results and discussion

1.1 Ion beam damage during milling as a factor in volumetric reconstruction: the possibility of ion-beam induced artefacts

In order to fully justify the contrast discussed above, two notes on possible artifacts, of either topographic or physico-chemical nature.
First, the possibility of inducing beam damage to the physic-chemical integrity of the matrix needs to be discussed, to rule out ion-beam artifacts producing the contrast we attribute to phase separation. On those lines, the effects of ion and electron beam irradiation in coal and polyacrylamide (PAAm) have been thoroughly discussed by way of synchrotron spectroscopies.[4] In their study, Bassim and coworkers reported physical buckling of thin PAAm slabs due to local heating. In addition, chemical changes were attributed to hydrogen loss. Coal showed little thermal or chemical effects from irradiation. The physical buckling, however, occurred during the last steps in the thinning process, on already nm-thin slabs. These effects would have no impact on the discussion above, since phase separation is already favoring atomic number contrast and, in the event of hydrogen loss in the polymeric blend, this would not originate a contrast mechanism in SE.

Finally, we need to address the possibility of ion beam milling-induced topographic defects throughout the cross-sectioning process. We wonder if such defects could be

the origin of dark and bright contrast that is currently being attributed to the presence of a labyrinth of pores within the fibers combined with phase separation.

In fact, Montecarlo and Molecular Dynamic simulations have confirmed surface amorphization damage of up to tens nms in Si.[5] These findings confirm the inability of ion milling to produce atomically flat surfaces (even when present as pre-existing condition). The question is whether this could translate into different sputtering rates, yielding a contrast map of PDMS/PMMA as a function of topography, rather than atomic number. However, this is unlikely. Topographic effects in the order of ten nanometers would be hardly resolved with our SE imaging settings.

Moreover, the question arises to whether pores in Figure 2 might be the result of accidental ion beam milling. However, Chen et al. had also observed development of pores in the films of IP networks,[6] as seen by SE upon surface fracture, i.e. in the absence of ion beam milling, which were attributed to loss of low molecular weight polymers during processing, through solvent extraction. We conclude our settings have provided a highly directional ion beam milling and regardless of the phase separation and milling efficiencies, the beam has been kept perpendicular to the surface vector at all times, providing clean, flush cross-sections consistently, not conducive to the accidental generation of the observed porous structure.

We then conclude that neither ion nor electron beam damage is responsible for any of the contrast discussed above.

1.2 Relative sign in Voltage Contrast

In terms of the relative signs of the contrast, Kovacs and coworkers identified the critical points E_1, and E_2 on the total electron emission yield as 1 and 2 keV respectively in their epoxy resins.[7] In this scheme, incident electron beam energies between 1 and 2 keV would charge up CNTs positive, and matrix negative. Whereas incident electron beams below E_1 and above E_2 correspond to negative charging of CNTs, yielding bright CNTs and dark matrix-consistent with our 3 keV energy beam. Although the precise values of E_1 and E_2 are system dependent, they will mostly depend on the electrical conductivity of the matrix, which are in both cases, good insulators. In our case, the beam energy was 3keV during image acquisition, and yields CNTs charging negative, suggesting that E_2 in PMMA is below 3keV.

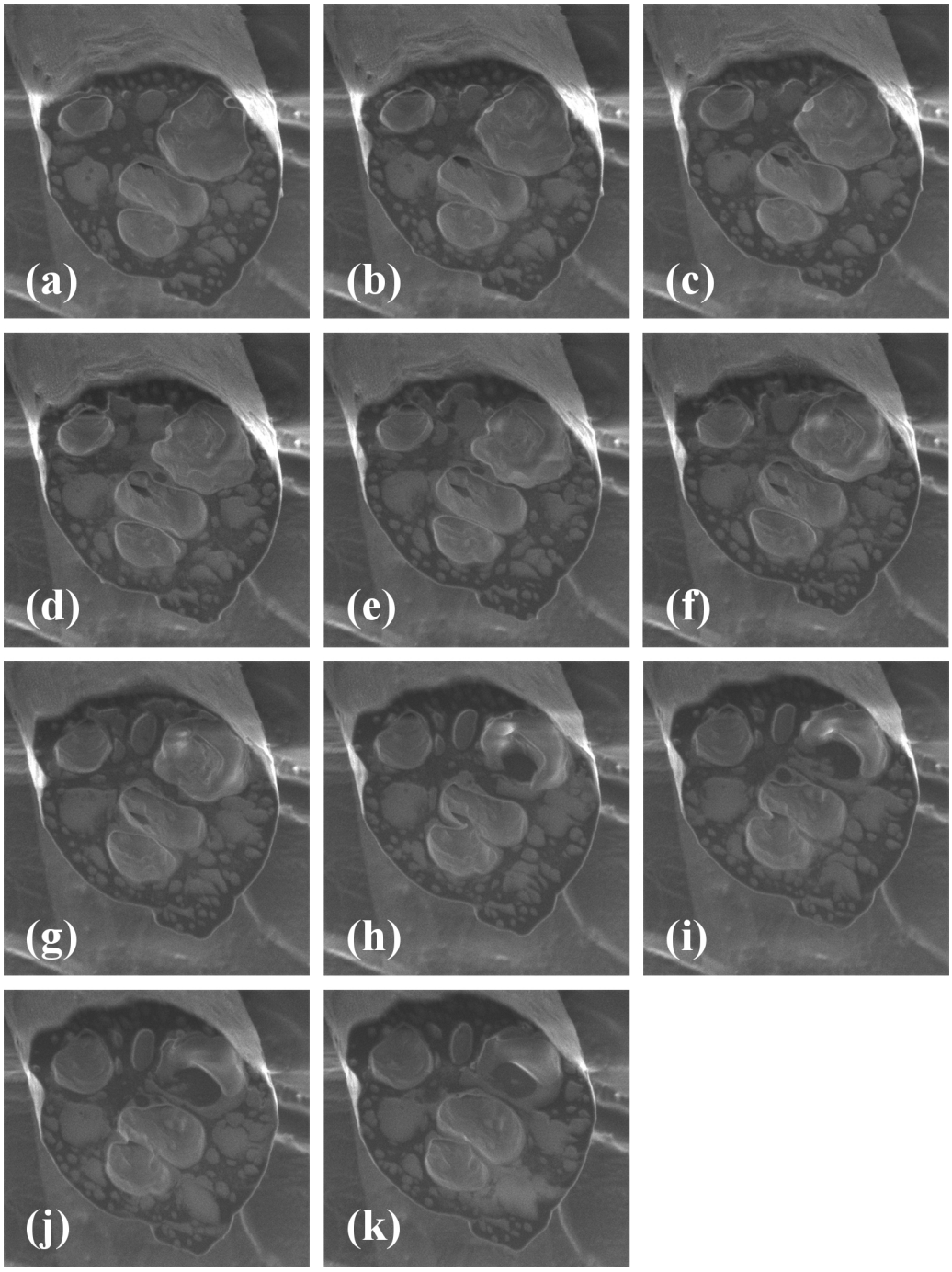

Figure S3: Library featuring all sequenced tomograms. Each tomogram appears without evidence of material-redeposition, promoting tomographic reconstruction.

1.3 Ion beam damage as a factor in CNT contrast interpretation

It is worth highlighting a number of processing elements have most likely altered the nominal conductivity of PMMA and of the composite altogether. Indeed, Winey and Fischer had reported increased bulk conductivity of up to 8 orders of magnitude upon the addition of CNT to the PMMA matrix.[8] In addition, ion beam irradiation has been reported to induce sp^2 hybridization, and hence, enhanced electrical conductivity

in polyamides.[9] This effect has been confirmed recently, through the observation of an enhanced NEXAFS π* C=C signal upon FIB milling followed by e-beam irradiation in PAAm.[4] Albeit, the overall conductivity increase reported by Winey and Fischer responded to measurements in the bulk, and the localized increased conductivity due to induced sp^2 hybridization. However, this modification is confined to the molecular realm, it clearly happens without detriment to the CNT/polymer interface sharp region of charge confinement, which is visible in the reconstructed volumes shown in Figure 3 a and b.

Supplementary Animation Sequences

SA1: Animation created by rotating around the x axis the reconstructed volume. (a) in greyscales and (b) in a colored scheme, where darker to bright contrast ranges from red to green.

SA2: Animation created by rotating around the y axis the reconstructed volume. (a) in greyscales and (b) in a colored scheme, where darker to bright contrast ranges from red to green.

[1] M. D. Uchic, L. Holzer, B. J. Inkson, E. L. Principe, P. Munroe, *MRS Bulletin* **2007**, *32*, 408.

[2] L. L. Arno P. Merkle, Andy Steinbach, Jeff Gelb, Martin Kienle, Michael W. Phaneuf, David Unrau, Sudhanshu S. Singh and Nikhilesh Chawla, *Microscopy and Analysis* **2014**, *7*, 10.

[3] L. Holzer, F. Indutnyi, P. Gasser, B. Münch, M. Wegmann, *Journal of Microscopy* **2004**, *216*, 84.

[4] N. Bassim, B. De Gregorio, A. Kilcoyne, K. Scott, T. Chou, S. Wirick, G. Cody, R. Stroud, *Journal of Microscopy* **2012**, *245*, 288.

[5] L. A. Giannuzzi, B. J. Garrison, *Journal of Vacuum Science & Technology A* **2007**, *25*, 1417.

[6] H. Chen, X. Deng, X. Hou, R. Luo, B. Liu, *Journal of Macromolecular Science, Part A* **2008**, *46*, 83.

[7] J. Z. Kovacs, K. Andresen, J. R. Pauls, C. P. Garcia, M. Schossig, K. Schulte, W. Bauhofer, *Carbon* **2007**, *45*, 1279.

[8] F. Du, J. E. Fischer, K. I. Winey, *Journal of Polymer Science Part B: Polymer Physics* **2003**, *41*, 3333.

[9] J. Davenas, G. Boiteux, *Adv. Mater.* **1990**, *2*, 521.